Research Article | Vol. 27, No. 19 / 16 September 2019 / Optics Express 27256
Optics EXPRESS

Passively mode-locked semiconductor quantum dot on silicon laser with 400 Hz RF line width

DOMINIK AUTH,[1] SONGTAO LIU,[2] JUSTIN NORMAN,[3] JOHN EDWARD BOWERS,[2] AND STEFAN BREUER[1,*]

[1]Institute of Applied Physics, Technische Universitat Darmstadt, Schloßgartenstraße 7, 64289 Darmstadt, Germany
[2]Department of Electrical and Computer Engineering, University of California Santa Barbara, Santa Barbara, California 93106, USA
[3]Materials Department, University of California Santa Barbara, Santa Barbara, California 93106, USA
[*]stefan.breuer@physik.tu-darmstadt.de

Abstract: Mode-locked InAs/InGaAs quantum dot lasers emitting optical frequency combs centered at 1310 nm are promising sources for high-speed and high-capacity communication applications. We report on the stable optical pulse train generation by a monolithic passively mode-locked edge-emitting two-section quantum dot laser based on a five-stack InAs/InGaAs dots-in-a-well structure directly grown on an on-axis (001) silicon substrate by solid-source molecular beam epitaxy. Optical pulses as short as 1.7 ps at a pulse repetition rate or inter-mode beat frequency of 9.4 GHz are obtained. A minimum pulse-to-pulse timing jitter of 9 fs, corresponding to a repetition rate line width of 400 Hz, is demonstrated. The generated optical frequency combs yield exceptional low amplitude jitter performance and comb widths exceed 5.5 nm at a −3 dB criteria, containing more than 100 comb carriers.

1. Introduction

Optical frequency comb passively mode-locked semiconductor quantum dot lasers directly grown on silicon are ideal sources for applications including high data rate optical communication applications in the O-band [1–5], spectroscopic sensing on a silicon photonics chip [6], dual-comb spectroscopy [7] and for silicon-chip based ultra-fast optical oscilloscopes [8]. Mode-locked quantum dot semiconductor lasers offer small size, higher functionality and lower energy consumption photonic integrated circuits on silicon, the material of choice for the photonics industry [2–4,9–15]. Ultra-fast optical pulse generation in quantum dot lasers benefits from broad gain spectra, due to the inhomogeneous broadening of the dots [16–18], ultra-fast carrier dynamics [19], modal gain saturating abruptly with carrier density [20,21] and easily saturable absorbers [22]. In optical communication systems, the pulse-to-pulse timing stability, equalling the full-width half-maximum of the inter-mode beat frequency line width, is a crucial parameter for switching operations between the data and control signal [23]. Since the first demonstration of light amplification and lasing in silicon by stimulated Raman scattering [24,25], the interest in light generation on silicon [26,27] has been strongly increasing. Lasing of self-organized quantum dots on silicon as dislocation filters have been demonstrated under pulsed mode in 2006 at an emission wavelength of 1100 nm and [28]. Continuous-wave laser emission by quantum dots at 1310 nm was demonstrated in 2010 by metal-organic chemical vapor deposition and layer-transfer onto a silicon substrate by GaAs/Si wafer bonding [29]. In 2011, continuous-wave laser emission by direct growth of quantum dots on a silicon (100) substrate emitting at 1310 nm has first been demonstrated [30]. Recently, a 6.7 mA record low threshold quantum dot laser on silicon with continuous-wave output has been shown [31]. In 2007 a monolithic passively mode-locked two-section quantum well laser was demonstrated on silicon via wafer bonding generating 4 ps short pulses at a repetition rate of 40 GHz [32]. Optical pulse train generation by a

#369251 https://doi.org/10.1364/OE.27.027256
Journal © 2019 Received 5 Jun 2019; revised 21 Jul 2019; accepted 8 Aug 2019; published 13 Sep 2019

Optics EXPRESS

passively mode-locked III-V on silicon quantum well laser with continuous-wave optical injection at 30 GHz repetition rate and with a repetition rate line width of 150 kHz was demonstrated where the pulse width had been derived to be 3 ps [33]. A tapered waveguide quantum well on silicon laser emitting optical pulse widths as low as 900 fs at a repetition rate of 20 GHz and 1.1 kHz line width has recently been reported [34]. First demonstration of passively mode-locking operation by a quantum dot laser directly grown on on-axis(001) silicon with pulse widths of 1.3 ps have been demonstrated at a repetition rate of 9.1 GHz and repetition rate line widths as narrow as 80 kHz [35]. In that work, saturable absorber section lengths from 3 % up to 23 % of the total laser length have been investigated and shorter pulses for longer absorber section lengths reported. Thus, a detailed analysis of the pulse train stability in terms of timing and amplitude jitter is still lacking. Subsequently, self mode-locking operation of a quantum dot on silicon laser without the need of any saturable absorber generated 490 fs short optical pulses has been reported at a repetition rate of 31 GHz and a repetition rate line width of 100 kHz [36]. The lowest repetition rate line width of a passively mode-locked quantum dot laser directly grown on silicon amounts to date to 1.8 kHz at a repetition rate of 20 GHz [1]. Shortest generated optical pulses from monolithic passively mode-locked quantum dot lasers grown on native substrates, except of silicon, are 360 fs [37] with a tapered waveguide design and 393 fs [38] for a two-section straight waveguide laser and 493 fs for a tapered three-section waveguide design [39]. Repetition rate line widths as low as 27 kHz [40], 23 kHz [39], 19 kHz [41], 18 kHz [42], 10 kHz [37], 2 kHz [43] and 500 Hz, with an amplitude jitter below 2 % for a packaged quantum dot mode-locked laser [44], have been reported [37–45]. Table 1 briefly summarizes reported performance of monolithic multi-section passively mode-locked quantum dot lasers highlighting shortest optical pulses and narrowest repetition rate line widths. The lowest reported values are highlighted bold. The first two references show the achieved results by the authors for quantum dot two-section devices directly grown on a silicon substrate.

Table 1. Performance of Monolithic Passively Mode-Locked Quantum Dot Lasers

Substrate	Repetition rate	Repetition rate line width	Pulse width	Year	Reference
Si	20 GHz	1.8 kHz	5 ps	2019	[1]
Si	9.1 GHz	80 kHz	1.3 ps	2018	[35]
GaAs	20 GHz	10 kHz	**360 fs**	2009	[37]
GaAs	21 GHz	-	393 fs	2007	[38]
GaAs	13 GHz	23 kHz	493 fs	2019	[39]
GaAs	5 GHz	27 kHz	10 ps	2010	[40]
GaAs	5 GHz	19 kHz	4 ps	2013	[41]
GaAs	16 GHz	18 kHz	1.4 ps	2015	[42]
GaAs	8 GHz	2 kHz	2 ps	2008	[43]
GaAs	10 GHz	**500 Hz**	4.5 ps	2009	[44]

In this contribution, the generation of stable optical pulse trains by a passively mode-locked InAs/InGaAs quantum dot laser directly grown on on-axis (100) silicon is demonstrated. Excellent pulse train timing and amplitude stability is demonstrated within a broad mode-locking area for the first time for these devices. The shortest pulses are 1.7 ps long. A lowest repetition rate line width of 400 Hz, corresponding to a pulse-to-pulse timing jitter of 9 fs at a repetition rate of 9.4 GHz, and an ultra-low relative amplitude jitter < 1 % is presented. Such low-noise compact monolithic ultra-fast laser source is promising for the integration in silicon based high-speed optical communication networks.

Optics EXPRESS

2. Device description and experimental set-up

The edge-emitting monolithic quantum dot laser consists of a five-stack InAs/InGaAs dots-in-a-well structure. Its epitaxial growth was completed on an on-axis (001) silicon substrate with a 45 nm GaP buffer layer by solid-source molecular beam epitaxy. Detailed epitaxial layer information and growth process information are covered in [35]. The total length of the laser was designed to be 4.5 mm with a saturable absorber section length corresponding to 18 % of the total laser length. The isolation length between gain and absorber section is 5 μm and the ridge width amounts to 3 μm. The laser is expected to emit picosecond short optical pulse trains at a fundamental repetition rate of 9.4 GHz corresponding to fundamental mode-locking as given by the free spectral range. The unpackaged laser device is placed on a copper mount which is temperature stabilized to a laser cooling block temperature of 20 °C and is contacted via an s-shaped fine probe tip with a point radius of 350 nm. A low-noise current source provides the laser gain injection current and a DC voltage source provides the reverse bias voltage to the absorber section. The laser pulse characteristics are investigated for increasing DC gain injection currents from 0 mA up to 160 mA in steps of 10 mA for each DC absorber reverse bias voltage ranging from 0 V up to 2.6 V in steps of 0.2 V. A schematic of the developed experimental emission characterization set-up is depicted in Fig. 1. The emitted laser light is coupled by a lensed single-mode fiber (coupling efficiency around 30 %). The fiber coupled optical power is depicted colour coded in Fig. 2(a) in dependence on the laser gain injection current and the absorber reverse bias voltage. To account for sufficient fiber-coupled optical power for nonlinear intensity auto-correlation and spectrally resolved measurements simultaneously, the light is amplified by a booster optical amplifier to several Milliwatt of average output power. The packaged commercial booster optical amplifier (Thorlabs, model: BOA1017) is kept constant at a temperature at 27 °C and driven by 600 mA gain injection current for all measurements. It has a length of 1.5 mm and a small signal gain around 27 dB. The amplified spontaneous emission spectrum is centered around 1300 nm and is exemplarily depicted in Fig. 2(b). Two optical fiber isolators with 32 dB isolation each are placed before and after the booster optical amplifier to prevent any unwanted residual optical feedback affecting the laser. The light is split by a fiber-based 50/50 beam-splitter where 50 % of the power is guided to a background-free nonlinear intensity auto-correlation technique with a high-sensitivity crystal for pulse width analysis. Optical pulse widths are determined by de-convoluting the full-width-at-half-maximum of Gaussian fit functions to the measured auto-correlation time traces. In the second branch of the fiber splitter, 50 % of the light is directed to a fast photo diode (electrical bandwidth 45 GHz) in combination with an electrical spectrum analyzer (electrical bandwidth 50 GHz) for radio-frequency analysis and to an optical spectrum analyzer (spectral resolution 10 pm) for optical spectra and bandwidth analysis. The timing stability of the optical pulse trains is quantified by the pulse-to-pulse timing jitter $\sigma_{\mathrm{ptp}} = (\Delta\nu/2\pi\nu_0^3)^{0.5}$ with ν_0 the fundamental repetition rate and $\Delta\nu$ the repetition rate line width [43]. The repetition rate line width is calculated from the timing phase noise power spectral density $L(f)$, given by $L(f) = \Delta\nu/2\pi f^2$ and is only valid for frequencies higher than $\Delta\nu/2$. In the measurements, the total timing phase noise power spectral density $L(f) = P(f - \nu_0)/(RBW \cdot P_{el,\,tot})$ [46] is composed of multiple separately measured power spectral densities each covering one order of frequency offset range where RBW is the resolution bandwidth of the electrical spectrum analyzer and $P_{el,\,tot}$ the total integrated power of the repetition rate line at ν_0. The final spectrum is obtained by linearly averaging 10 measured spectra with the detection mode of the electrical spectrum analyzer set to sample-mode [41]. The amplitude jitter of the optical pulse trains is quantified as a relative standard deviation of the pulse intensity variations determined by the ratio of the integrated power spectral density in the radio-frequency spectrum up to half the repetition rate and the power spectral density of the repetition rate peak [47].

Optics EXPRESS

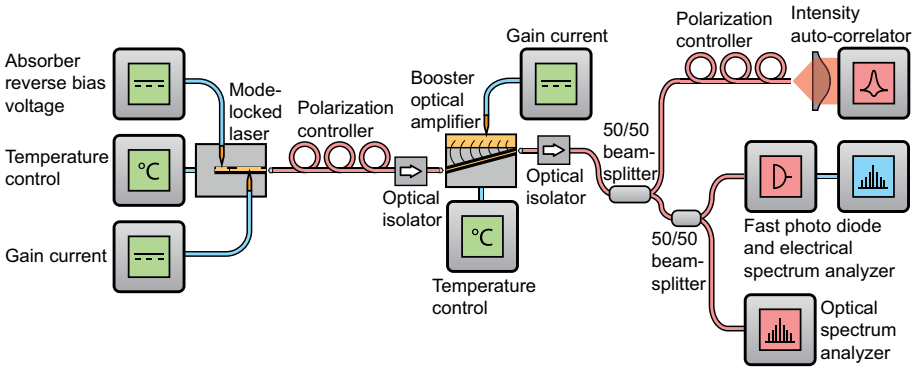

Fig. 1. Schematic of the measurement set-up. The laser emission is fiber-coupled and amplified by a booster optical amplifier and then analyzed by an intensity auto-correlator, fast-photodiode and electrical spectrum analyzer and an optical spectrum analyzer.

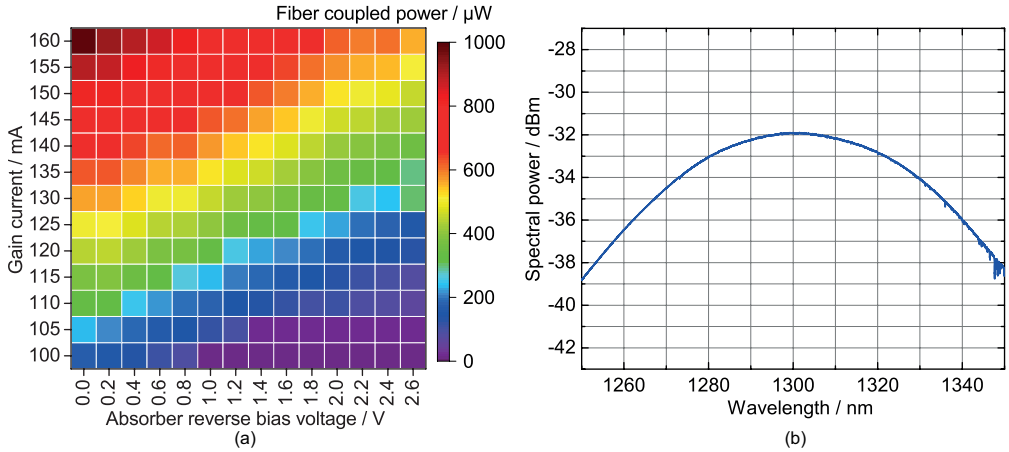

Fig. 2. (a) Average fiber coupled optical power of the passively mode-locked laser before entering the booster optical amplifier. The coupling efficiency is around 30 %. (b) Spectrum of the amplified spontaneous emission solely by the booster optical amplifier at 600 mA and 27 °C centered around 1300 nm. The −3dB spectral width is 67 nm.

3. Mode-locking pulse train and stability characterization

In the following, we present the radio-frequency domain, optical and time domain characteristics of the laser. At first, the fundamental mode-locking beat frequency peak signal-to-noise ratio in the radio-frequency domain is investigated in dependence on the laser gain injection current and the applied absorber reverse bias voltage. The experimental results are depicted color-coded in Fig. 3(a). Overall, a radio-frequency peak signal-to-noise ratio exceeding 30 dB is found for almost the entire area of bias conditions. The highest radio-frequency signal-to-noise ratio is found in an area bounded by white dashes, denoted by A. The maximum ratio of 59 dB is found at a gain current of 160 mA and for a reverse bias voltage of 1.4 V. For gain currents above 145 mA and for absorber reverse bias voltages above 1.8 V, splitting of the optical spectra occur with a mode group spectral separation of 7 nm and lower radio-frequency peak signal-to-noise ratios than these identified in area A. This dual-mode group lasing appears common for quantum dot lasers as the carriers are localized in different dots that may be unable to interact directly, resulting in a system without a global Fermi function and exhibiting an inhomogeneously broadened gain spectra

Optics EXPRESS

[16,48,49]. For gain currents from 120 mA up to 145 mA and reverse bias voltages above 1.8 V, low radio-frequency signal-to-noise ratios are found. This area is marked with a white dashed line and denoted as area B, indicating less stable mode-locking operation. This is supported by the absence of optical pulses in the auto-correlation spectra in area B. A representative measured radio-frequency trace is depicted in Fig. 3(b) for 120 mA and 2.6 V. The fundamental repetition rate of 9.4 GHz, corresponding to the free spectral range of the passively mode-locked quantum dot laser, higher harmonics with descending peak power as well as the absence of low-frequency fluctuations or Q-switched mode-locking are indicated [46].

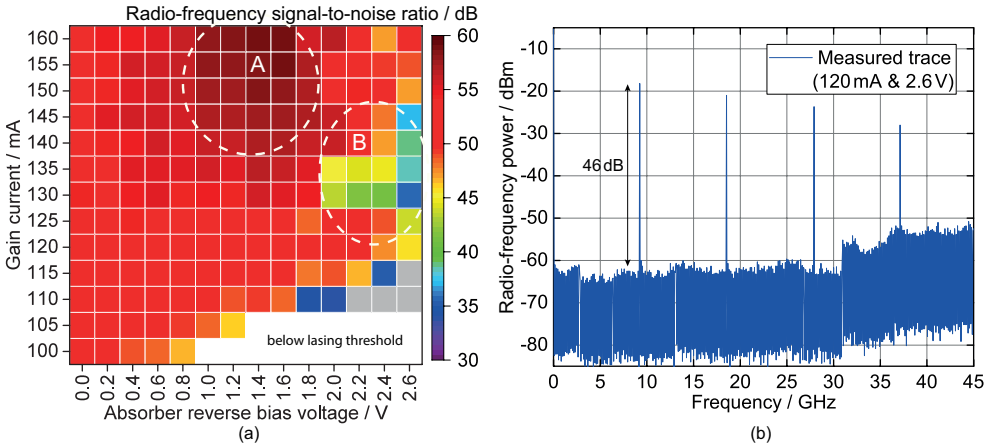

Fig. 3. (a) Color-coded fundamental mode-locking beat frequency peak signal-to-noise ratio in dependence on the absorber reverse bias voltage and the gain current. A large mode-locking area with ratios >50 dB is obtained. The maximum ratio of 59 dB is found at a gain current of 160 mA and 1.4 V reverse bias voltage. In the gray area, above lasing threshold, and at high reverse bias voltages, radio-frequency peak signal-to-noise ratio less than 30 dB result. (b) Selected radio-frequency spectrum acquired at an injection current of 120 mA and at an applied absorber reverse bias voltage of 2.6 V and indicated within a frequency span of 45 GHz.

The optical pulse widths are determined by a background-free non-linear intensity auto-correlation technique with a high-sensitivity crystal by de-convolution of Gaussian fits to the auto-correlation signal, and results are depicted color-coded in Fig. 4(a). In the gray colored area, absorption prevails and hence no lasing or pulse generation occurs. At the majority of operation points in the map however, clean Gaussian shaped auto-correlation time traces are obtained. Example traces are depicted in Fig. 4(b) for different bias conditions. Above lasing threshold, the shortest pulses are found and this area is indicated with a white dashed line denoted as area D. A shortest pulse width of 1.7 ps is recorded at 120 mA and at 2.6 V and the corresponding auto-correlation time-trace including a Gaussian fit is depicted in the bottom left corner of Fig. 4(b). This corresponds to a pulse peak power of 28.2 mW taking into account a pulse-shape-factor of 0.94 for Gaussian pulses [42] at an average optical output power of 0.48 mW solely by the passively mode-locked laser. This pulse width for a quantum dot laser on silicon is narrow, however 4.8 times larger than that for a tapered design on GaAs [37]. Additionally, in area D, the pulse widths are slightly decreasing with increasing absorber reverse bias voltage due to the higher pulse shortening effect of the stronger absorption and the pulses broaden with increasing gain current. Besides the short pulses the broadest optical spectra are obtained as well in area D. At low absorber reverse bias voltages and at high gain currents, pulse widths ranging from 10 ps up to 30 ps are obtained in an area denoted as area C, indicated by a white dashed line. In area C coherence artifacts with auto-correlation amplitudes equal to the ones of the Gaussian

Optics EXPRESS

background signal can arise in the auto-correlation time traces. An example auto-correlation time trace for area C is depicted in the top left corner of Fig. 4(b). For higher gain injection currents above 160 mA area C is expanding towards higher absorber reverse bias voltages above 0.8 V.

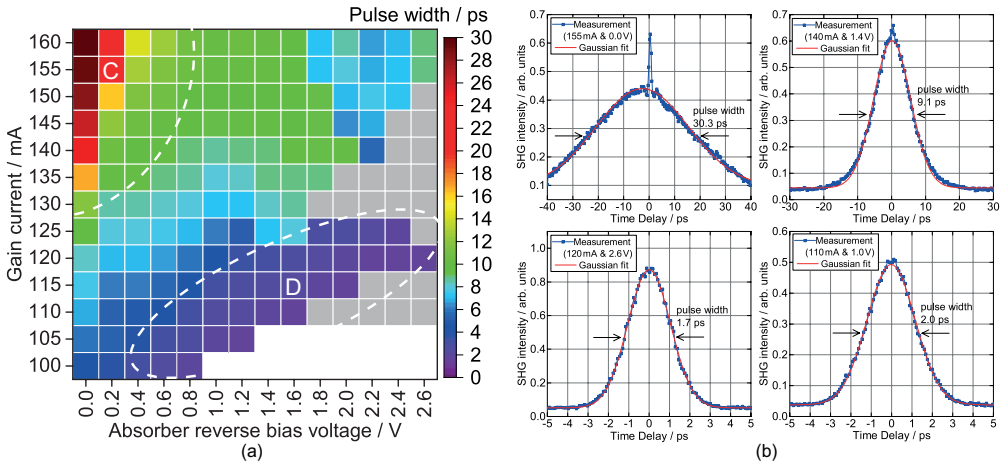

Fig. 4. (a) Color-coded de-convoluted pulse width in dependence on gain current and absorber reverse bias voltage. Gray: continuous-wave emission. (b) Example auto-correlation time traces with Gaussian fits. The shortest pulse width of 1.7 ps is depicted in the left bottom corner found at an injection current of 120 mA and an absorber reverse bias voltage of 2.6 V. In the top left corner at 155 mA and 0.0 V a strong coherent spike on top of the Gaussian pulse is found what is ignored for the Gaussian fit.

The −3 dB optical spectra widths, generated in dependence on the gain current and absorber reverse bias voltage, are depicted color-coded in Fig. 5(a). In area D, the broadest optical spectra widths or optical frequency combs are found, in accordance with the shortest optical pulses in Fig. 4(a). Here, comb widths range from 1.1 nm (110 mA, 1.8 V) up to a maximum of 5.5 nm (115 mA, 1.0 V). This corresponds to a maximum of 103 optical lines or comb carriers within the −3 dB spectral width. The corresponding spectrum is depicted in the top left corner of Fig. 5(b). Outside of area D, the comb widths are mostly below 0.5 nm. An example spectrum is shown in the top right corner of Fig. 5(b). As indicated earlier, at high gain currents and high absorber reverse bias voltages in area E a splitting of the optical spectrum can occur. An example trace is depicted in the bottom right corner of Fig. 5(b). For higher gain injection currents than 160 mA area E is expanding to lower absorber reverse bias voltages below 1.8 V. The bottom left corner shows the attained optical comb centered at 1312.5 nm yielding a comb width of 2.63 nm corresponding to the shortest pulses at 120 mA and 2.6 V. This results in a time-bandwidth-product of 0.78 being only 1.77 times higher than the time-bandwidth-product for Fourier-limited Gaussian pulses of 0.44. This time-bandwidth-product value indicates a small amount of chirping within the optical pulse.

A map of the estimated time-bandwidth-product is depicted color-coded in Fig. 6(a) in dependence on the injected gain currents and applied absorber reverse bias voltages. Within area D of the shortest optical pulses, the time-bandwidth-product ranges from 0.7 (100 mA, 0.8 V) up to 3.1 (115 mA, 1.0 V). This indicates that a fraction of the modes in the −3 dB spectral width are locked and the pulse is slightly chirped. For the majority of laser biasing conditions, the optical pulses are nearly Fourier-limited, indicated by the wide purple area, except for gain currents above 135 mA and reverse bias voltages below 0.4 V in area C. There, time-bandwidth-products exceeding 4.4 are found which are attributed to less stable mode-locking due to the low absorber reverse bias voltage. In that area, coherent artifacts can be found in the auto-correlation time

Optics EXPRESS

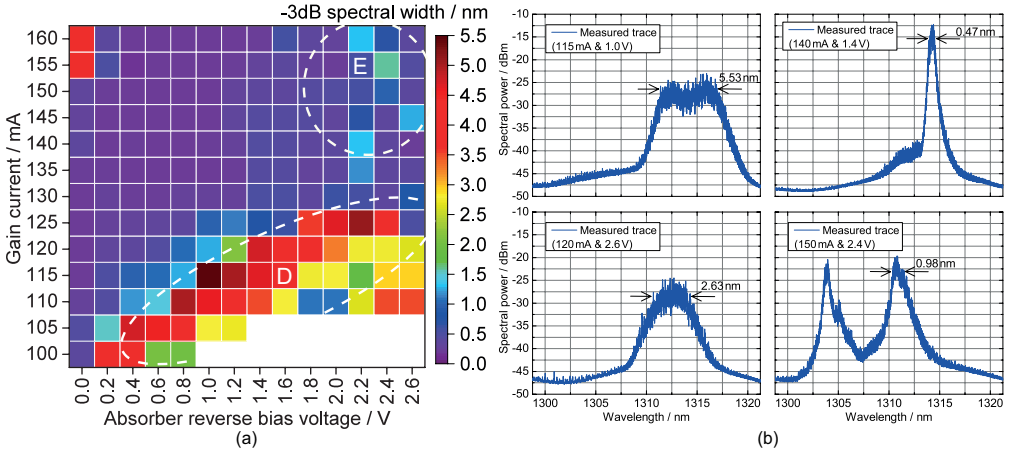

Fig. 5. (a) Color-coded −3 dB spectral width in dependence on gain c reverse bias voltage. (b) Example optical spectra for different bias conditions. The bottom left corner shows the spectrum for an injection current of 120 mA and an absorber reverse bias voltage of 2.6 V at the shortest pulse width of 1.7 ps depicting a −3dB spectral width of 2.63 nm.

traces with amplitudes larger than the Gaussian background. Since the booster optical amplifier is not impacting the −3 dB optical width of the passively mode-locked laser, it can be concluded from the large purple area in Fig. 6(a) for the time bandwidth product showing values of 0.44 that the booster optical amplifier in this area is not broadening the optical pulses. Only in area D larger time bandwidth products are obtained. Here, a comparative measurement with and without booster optical amplifier of the pulse width is not possible due to too low optical output powers in this area for nonlinear intensity auto-correlation.

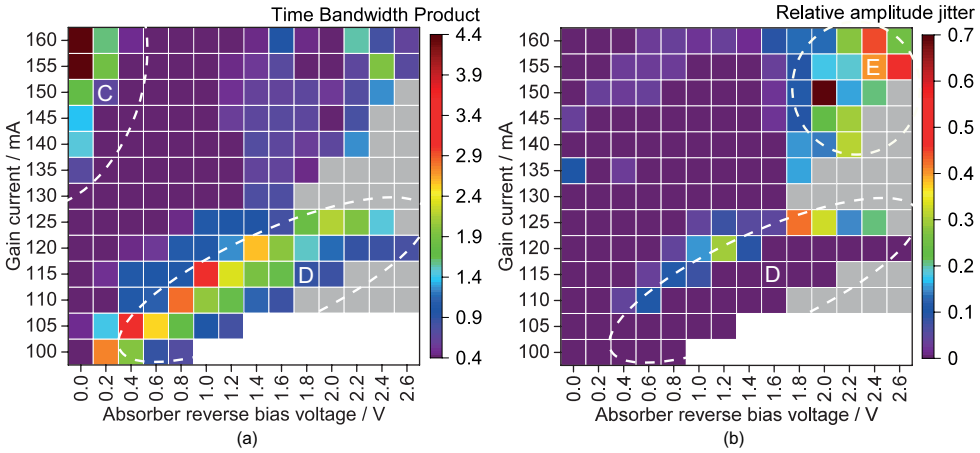

Fig. 6. (a) Color-coded time bandwidth product and (b) color-coded relative amplitude jitter in dependence on the absorber reverse bias voltage and the gain current.

In the following, we aim to study the low-frequency noise or amplitude noise of the generated pulse trains, in particular to identify possible amplitude modulated pulse regimes. Therefore, we quantify and depict the measured relative amplitude jitter in Fig. 6(b). As indicated in Fig. 6(b), amplitude jitter below 1 % is attained in area D where the shortest pulses are identified (color coded purple). Such low amplitude jitter denotes excellent stable passive mode-locking operation.

Optics EXPRESS

In contrast, at high gain currents above 135 mA and high absorber reverse bias voltages above 1.8 V in area E, strong relative amplitude jitter values are found ranging from 15 % up to 70 %. This indicates unstable mode-locking operation possibly caused by the second mode group appearing in the optical spectra in this area.

The pulse-to-pulse timing jitter is depicted in Fig. 7(a) in dependence on the laser gain current and absorber reverse bias voltage. Low timing jitter values of around 100 fs to 200 fs can be identified in the majority of biasing areas. In area A, where the highest radio-frequency peak signal-to-noise ratios are found, timing jitter values range between 65 fs and 150 fs. Area C depicts timing jitter values up to 650 fs where also coherent artifacts appear in the auto-correlation traces and their widths can be related to the pulse coherence time and indicate the shortest temporal structure in the pulse intensity [50]. In the regime with low timing jitter values, indicating stable mode-locking, these artifacts are absent. In area E, the timing jitter increases up to values above 800 fs, corresponding to repetition rate line widths beyond 3 MHz, what is also denoted as unstable mode-locking, yet no artifacts appear in that area. This additional noise contribution is attributed to the second mode group identified in the optical domain within area E. In area D, located just above lasing threshold and at gain currents below 125 mA, where also the shortest pulses where found, timing jitter values are below 50 fs, indicated by purple color coding. A lowest timing jitter of 9 fs, corresponding to a fundamental repetition rate −3 dB line width or inter-mode beat line width of 400 Hz is identified at a gain current of 105 mA and an absorber reverse bias voltage of 0.6 V. The corresponding timing phase noise power spectral density spectrum $L(f)$ is depicted in Fig. 7(b) together with a 400 Hz line which may serve as a guide to the eye. The phase noise clearly follows the 400 Hz up to an offset frequency of 10 MHz. At 10 MHz and −120 dBc/Hz the baseline of the electrical spectrum analyzer is reached. Measurements without the use of the booster optical amplifier have shown that neither the −3 dB spectral width nor the timing jitter is influenced by the booster optical amplifier, only the baseline for L(f) at −120 dBc/Hz is increasing due to the lower power impinging onto the detector. The lowest identified value of 9 fs for the pulse-to-pulse timing jitter for this laser is 1.5 times higher than the one for the lowest timing jitter obtained so far by a passively mode-locked quantum dot laser on silicon of 6 fs at 20 GHz with a 1.6 times broader pulse width at this operation point [1] than the device presented in this work.

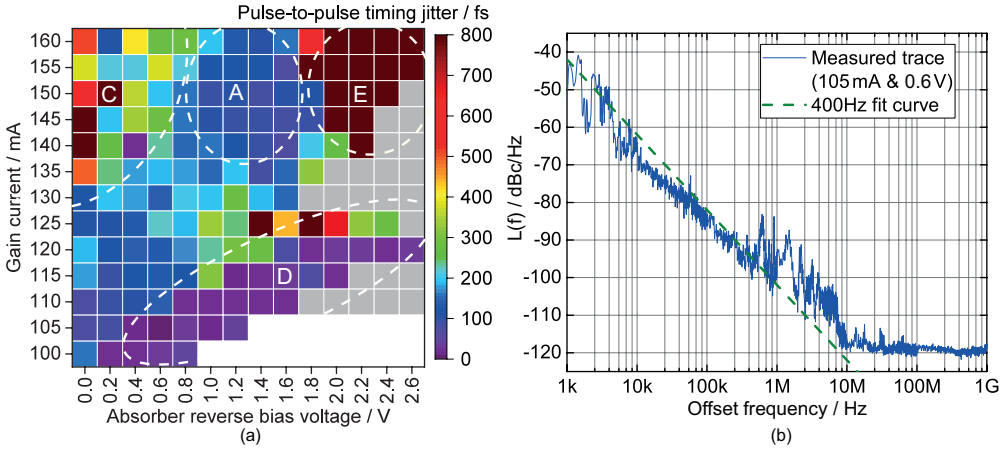

Fig. 7. (a) Color-coded pulse-to-pulse timing jitter in dependence on the absorber reverse bias voltage and the gain current. (b) Example timing phase noise power spectral density trace $L(f)$ for 105 mA and 0.6 V where the lowest timing jitter of 9 fs is found. This trace belongs to a repetition rate line width of 400 Hz plotted with a green dashed line as guide to the eye.

Optics EXPRESS

Finally, Table 2 summarizes the three highlighted laser biasing conditions for optimum timing jitter, pulse width, −3 dB spectral width and corresponding obtained values for the time bandwidth product, average optical output power and pulse peak power. All three operation points are located in area D. The best values are highlighted in bold. In literature, line widths of 100 kHz (−3 dB) for a self mode-locked quantum dot laser on silicon [36] and 80 kHz for a similar device presented here [35] were reported indicating a 200-250 times broader repetition rate line width as compared to the here presented results although no precise pulse train stability analysis in terms of radio-frequency line width has been carried out yet for these devices. Additionally, in the results presented here, a 2.75 times narrower repetition rate line width is observed as compared to the reported repetition rate line width of 1.1 kHz from a complex tapered waveguide design from a silicon quantum-well laser [34] and 4.5 times narrower line width compared to the 1.8 kHz width reported for a monolithic InAs quantum dot passively mode-locked two-section laser on silicon [1]. Comparing the achieved timing stability with quantum dot passively mode-locked lasers on native substrates, except of silicon, repetition rate line widths ranging from 500 Hz up to 27 kHz [37,39–43] have been reported. A 1.25 to 67.5 times narrower line width is presented here. Compared to the lowest value of 500 Hz at 10 GHz by a packaged quantum dot laser presented in [44] the here presented laser still shows a higher pulse train timing stabiliy. Pulse train amplitude stability studies are performed relatively scarcely. In [51] a stable mode-locking area had recently been defined with relative amplitude jitter values below 6 % where higher values had been connected to leading edge or trailing edge pulse instabilities. Additionally in [44] an amplitude jitter to 1.2 % or around 1 % [37] has been presented. Except within area E, the here presented laser shows a considerably reduced relative amplitude jitter below 1 % in the majority of gain injection currents and absorber reverse bias voltages indicating ultra-stable pulse amplitude stability.

Table 2. Best Values of Characteristic Laser Parameters

Gain injection current	105 mA	115 mA	120 mA
Absorber reverse bias voltage	0.6 V	1.0 V	2.6 V
Pulse width	3.2 ps	3.2 ps	**1.7 ps**
Pulse-to-pulse timing jitter	**9 fs**	317 fs	28 fs
Repetition rate line width	**400 Hz**	520 kHz	4 kHz
−3 dB spectral width	4.5 nm	**5.5 nm**	2.6 nm
Time bandwidth product	2.52	3.10	0.78
Average optical output power	0.64 mW	0.89 mW	0.48 mW
Pulse peak power	19.9 mW	27.9 mW	28.2 mW

4. Conclusion

Stable optical pulse trains have been generated by a monolithic passively mode-locked InAs/InGaAs quantum dot laser directly grown on silicon. The lowest optical pulse width amounted to 1.7 ps, the lowest pulse-to-pulse timing jitter to 9 fs, corresponding to a repetition rate or inter-mode beat line width of 400 Hz. A relative amplitude jitter below 1 % at a repetition rate of 9.4 GHz indicated exceptionally stable pulse train generation. A broad emission area has been identified just above lasing threshold where the amplitude jitter was well below 1 %, the timing jitter below 50 fs and the optical pulse widths below 3 ps. The laser generated optical frequency combs spanning 5.5 nm within a −3 dB bandwidth and containing more than 100 comb carriers. The monolithic passively mode-locked two-section quantum dot laser should serve as a promising source for future large-scale high capacity silicon photonic integrated circuits where ultra-stable optical pulse operation is critically demanded.

Optics EXPRESS

Funding

U.S. Department of Energy Advanced Research Projects Agency-Energy (DE-AR000067); ENLITENED Program, Advanced Research Projects Agency-Energy (ARPA-E) (DE-AR0000843); German Research Foundation (DFG) (389193326); Open Access Publishing Fund of Technische Universität Darmstadt; Adolf Messer Foundation.

References

1. S. Liu, X. Wu, D. Jung, J. C. Norman, M. J. Kennedy, H. K. Tsang, A. C. Gossard, and J. E. Bowers, "High-channel-count 20 GHz passively mode-locked quantum dot laser directly grown on Si with 4.1 Tbit/s transmission capacity," Optica **6**(2), 128–134 (2019).
2. J. C. Norman, D. Jung, Z. Zhang, Y. Wan, S. Liu, C. Shang, R. W. Herrick, W. W. Chow, A. C. Gossard, and J. E. Bowers, "A review of high-performance quantum dot lasers on silicon," IEEE J. Quantum Electron. **55**(2), 1–11 (2019).
3. R. Jones, P. Doussiere, J. B. Driscoll, W. Lin, H. Yu, Y. Akulova, T. Komljenovic, and J. E. Bowers, "Heterogeneously integrated InP/Silicon photonics: Fabricating fully functional transceivers," IEEE Nanotechnology Mag. **13**(2), 17–26 (2019).
4. R. Helkey, A. A. M. Saleh, J. Buckwalter, and J. E. Bowers, "High-Performance Photonic Integrated Circuits on Silicon," IEEE J. Sel. Top. Quantum Electron. **25**(5), 1–15 (2019).
5. S. Chen, M. Tang, S. Shutts, S. Elliott, A. Sobiesierski, I. Ross, P. Smowton, A. Seeds, and H. Liu, "Electrically pumped continuous-wave III–V quantum dot lasers monolithically grown on silicon," in "*2016 International Semiconductor Laser Conference (ISLC)*," pp. 1–2 (2016).
6. A. Z. Subramanian, E. Ryckeboer, A. Dhakal, F. Peyskens, A. Malik, B. Kuyken, H. Zhao, S. Pathak, A. Ruocco, A. D. Groote, P. Wuytens, D. Martens, F. Leo, W. Xie, U. D. Dave, M. Muneeb, P. V. Dorpe, J. V. Campenhout, W. Bogaerts, P. Bienstman, N. L. Thomas, D. V. Thourhout, Z. Hens, G. Roelkens, and R. Baets, "Silicon and silicon nitride photonic circuits for spectroscopic sensing on-a-chip [Invited]," Photonics Res. **3**(5), B47–B59 (2015).
7. B. Bernhardt, A. Ozawa, P. Jacquet, M. Jacquey, Y. Kobayashi, T. Udem, R. Holzwarth, G. Guelachvili, T. W. Hansch, and N. Picqué, "Cavity-enhanced dual-comb spectroscopy," Nat. Photonics **4**(1), 55–57 (2010).
8. M. A. Foster, R. Salem, D. F. Geraghty, A. C. Turner-Foster, M. Lipson, and A. L. Gaeta, "Silicon-chip-based ultrafast optical oscilloscope," Nature **456**(7218), 81–84 (2008).
9. D. Bimberg, M. Kuntz, and M. Laemmlin, "Quantum dot photonic devices for lightwave communication," Microelectron. J. **36**(3-6), 175–179 (2005).
10. D. Bimberg, G. Fiol, M. Kuntz, C. Meuer, M. Lammlin, N. Ledentsov, and A. Kovsh, "High speed nanophotonic devices based on quantum dots," Phys. Status Solidi A **203**(14), 3523–3532 (2006).
11. J. C. Norman, D. Jung, Y. Wan, and J. E. Bowers, "Perspective: The future of quantum dot photonic integrated circuits," APL Photonics **3**(3), 030901 (2018).
12. Z. Lu, J. Jhoja, J. Klein, X. Wang, A. Liu, J. Flueckiger, J. Pond, and L. Chrostowski, "Performance prediction for silicon photonics integrated circuits with layout-dependent correlated manufacturing variability," Opt. Express **25**(9), 9712–9733 (2017).
13. G. Roelkens, L. Liu, D. Liang, R. Jones, A. Fang, B. Koch, and J. Bowers, "III-V/silicon photonics for on-chip and intra-chip optical interconnects," Laser Photonics Rev. **4**(6), 751–779 (2010).
14. B. Jalali and S. Fathpour, "Silicon Photonics," J. Lightwave Technol. **24**(12), 4600–4615 (2006).
15. A. W. Fang, H. Park, O. Cohen, R. Jones, M. J. Paniccia, and J. E. Bowers, "Electrically pumped hybrid AlGaInAs-silicon evanescent laser," Opt. Express **14**(20), 9203–9210 (2006).
16. L. V. Asryan and R. Suris, "Inhomogeneous line broadening and the threshold current density of a semiconductor quantum dot laser," Semicond. Sci. Technol. **11**(4), 554–567 (1996).
17. M. Kuntz, G. Fiol, M. Laemmlin, C. Meuer, and D. Bimberg, "High-speed mode-locked quantum-dot lasers and optical amplifiers," Proc. IEEE **95**(9), 1767–1778 (2007).
18. W. W. Chow, A. Y. Liu, A. C. Gossard, and J. E. Bowers, "Extraction of inhomogeneous broadening and nonradiative losses in InAs quantum-dot lasers," Appl. Phys. Lett. **107**(17), 171106 (2015).
19. P. Borri, S. Schneider, W. Langbein, and D. Bimberg, "Ultrafast carrier dynamics in InGaAs quantum dot materials and devices," J. Opt. A: Pure Appl. Opt. **8**(4), S33–S46 (2006).
20. J. K. Mee, R. Raghunathan, J. B. Wright, and L. F. Lester, "Device geometry considerations for ridge waveguide quantum dot mode-locked lasers," J. Phys. D: Appl. Phys. **47**(23), 233001 (2014).
21. D. R. Matthews, H. D. Summers, P. M. Smowton, and M. Hopkinson, "Experimental investigation of the effect of wetting-layer states on the gain-current characteristic of quantum-dot lasers," Appl. Phys. Lett. **81**(26), 4904–4906 (2002).
22. E. Rafailov, M. Cataluna, and E. A. Avrutin, *Quantum Dot Saturable Absorbers* (John Wiley & Sons, Ltd, 2011), Chap. 4, pp. 77–97.
23. D. Zibar, L. K. Oxenlowe, H. C. H. Mulvad, J. Mork, M. Galili, A. T. Clausen, and P. Jeppesen, "The Effect of Timing Jitter on a 160-Gb/s Demultiplexer," IEEE Photonics Technol. Lett. **19**(13), 957–959 (2007).
24. O. Boyraz and B. Jalali, "Demonstration of a silicon Raman laser," Opt. Express **12**(21), 5269–5273 (2004).

Optics EXPRESS

25. H. Rong, R. Jones, A. Liu, O. Cohen, D. Hak, A. Fang, and M. Paniccia, "A continuous-wave Raman silicon laser," Nature **433**(7027), 725–728 (2005).
26. D. Liang and J. Bowers, "Recent progress in lasers on silicon," Nat. Photonics **4**(8), 511–517 (2010).
27. Z. Wang, A. Abbasi, U. Dave, A. De Groote, S. Kumari, B. Kunert, C. Merckling, M. Pantouvaki, Y. Shi, B. Tian, K. Van Gasse, J. Verbist, R. Wang, W. Xie, J. Zhang, Y. Zhu, J. Bauwelinck, X. Yin, Z. Hens, J. Van Campenhout, B. Kuyken, R. Baets, G. Morthier, D. Van Thourhout, and G. Roelkens, "Novel Light Source Integration Approaches for Silicon Photonics," Laser Photonics Rev. **11**(4), 1700063 (2017).
28. Z. Mi, J. Yang, P. Bhattacharya, and D. L. Huffaker, "Self-organised quantum dots as dislocation filters: the case of GaAs-based lasers on silicon," Electron. Lett. **42**(2), 121–123 (2006).
29. K. Tanabe, D. Guimard, D. Bordel, S. Iwamoto, and Y. Arakawa, "Electrically pumped 1.3 μm room-temperature InAs/GaAs quantum dot lasers on Si substrates by metal-mediated wafer bonding and layer transfer," Opt. Express **18**(10), 10604–10608 (2010).
30. T. Wang, H. Liu, A. Lee, F. Pozzi, and A. Seeds, "1.3-μm InAs/GaAs quantum-dot lasers monolithically grown on Si substrates," Opt. Express **19**(12), 11381–11386 (2011).
31. D. Jung, J. Norman, M. J. Kennedy, C. Shang, B. Shin, Y. Wan, A. C. Gossard, and J. E. Bowers, "High efficiency low threshold current 1.3 μm InAs quantum dot lasers on on-axis (001) GaP/Si," Appl. Phys. Lett. **111**(12), 122107 (2017).
32. B. R. Koch, A. W. Fang, O. Cohen, and J. E. Bowers, "Mode-locked silicon evanescent lasers," Opt. Express **15**(18), 11225–11233 (2007).
33. Y. Cheng, X. Luo, J. Song, T.-Y. Liow, G.-Q. Lo, Y. Cao, X. Hu, X. Li, P. H. Lim, and Q. J. Wang, "Passively mode-locked III-V/silicon laser with continuous-wave optical injection," Opt. Express **23**(5), 6392–6399 (2015).
34. M. L. Davenport, S. Liu, and J. E. Bowers, "Integrated heterogeneous silicon/III-V mode-locked lasers," Photonics Res. **6**(5), 468–478 (2018).
35. S. Liu, J. Norman, D. Jung, M. Kennedy, A. C Gossard, and J. Bowers, "Monolithic 9 GHz passively mode locked quantum dot lasers directly grown on on-axis (001) Si," Appl. Phys. Lett. **113**(4), 041108 (2018).
36. S. Liu, D. Jung, J. C. Norman, M. J. Kennedy, A. C. Gossard, and J. E. Bowers, "490 fs pulse generation from passively mode-locked single section quantum dot laser directly grown on on-axis GaP/Si," Electron. Lett. **54**(7), 432–433 (2018).
37. M. G. Thompson, A. R. Rae, M. Xia, R. V. Penty, and I. H. White, "InGaAs Quantum-Dot Mode-Locked Laser Diodes," IEEE J. Sel. Top. Quantum Electron. **15**(3), 661–672 (2009).
38. E. Rafailov, M. Cataluna, and W. Sibbett, "Mode-locked quantum-dot lasers," Nat. Photonics **1**(7), 395–401 (2007).
39. S. Meinecke, L. Drzewietzki, C. Weber, B. Lingnau, S. Breuer, and K. Ludge, "Ultra-Short Pulse Generation in a Three Section Tapered Passively Mode-Locked Quantum-Dot Semiconductor Laser," Sci. Rep. **9**(1), 1783 (2019).
40. C.-Y. Lin, F. Grillot, Y. Li, R. Raghunathan, and L. F. Lester, "Characterization of timing jitter in a 5 GHz quantum dot passively mode-locked laser," Opt. Express **18**(21), 21932–21937 (2010).
41. L. Drzewietzki, S. Breuer, and W. Elsäßer, "Timing jitter reduction of passively mode-locked semiconductor lasers by self- and external-injection: Numerical description and experiments," Opt. Express **21**(13), 16142–16161 (2013).
42. C. Weber, L. Drzewietzki, M. Rossetti, T. Xu, P. Bardella, H. Simos, C. Mesaritakis, M. Ruiz, I. Krestnikov, D. Livshits, M. Krakowski, D. Syvridis, I. Montrosset, E. U. Rafailov, W. Elsaßer, and S. Breuer, "Picosecond pulse amplification up to a peak power of 42 W by a quantum-dot tapered optical amplifier and a mode-locked laser emitting at 1.26 μm," Opt. Lett. **40**(3), 395–398 (2015).
43. F. Kefelian, S. O'Donoghue, M. T. Todaro, J. G. McInerney, and G. Huyet, "RF Linewidth in Monolithic Passively Mode-Locked Semiconductor Laser," IEEE Photonics Technol. Lett. **20**(16), 1405–1407 (2008).
44. G. Carpintero, M. G. Thompson, R. V. Penty, and I. H. White, "Low noise performance of passively mode-locked 10-ghz quantum-dot laser diode," IEEE Photonics Technol. Lett. **21**(6), 389–391 (2009).
45. H. Schmeckebier, G. Fiol, C. Meuer, D. Arsenijević, and D. Bimberg, "Complete pulse characterization of quantum-dot mode-locked lasers suitable for optical communication up to 160 Gbit/s," Opt. Express **18**(4), 3415–3425 (2010).
46. D. von der Linde, "Characterization of the noise in continuously operating mode-locked lasers," Appl. Phys. B: Lasers Opt. **39**(4), 201–217 (1986).
47. C. Weber, A. Klehr, A. Knigge, and S. Breuer, "Picosecond Pulse Generation and Pulse Train Stability of A Monolithic Passively Mode-Locked Semiconductor Quantum-Well Laser at 1070 nm," IEEE J. Quantum Electron. **54**(3), 1–9 (2018).
48. M. Grundmann and D. Bimberg, "Gain and threshold of quantum dot lasers: Theory and comparison to experiments," Jpn. J. Appl. Phys. **36**(6B), 4181–4187 (1997).
49. L. Harris, D. J. Mowbray, M. S. Skolnick, M. Hopkinson, and G. Hill, "Emission spectra and mode structure of InAs/GaAs self-organized quantum dot lasers," Appl. Phys. Lett. **73**(7), 969–971 (1998).
50. H. Weber, "Comments on the pulse width measurement with two-photon excitation of fluorescence," Phys. Lett. A **27**(5), 321–322 (1968).
51. P. Bardella, L. Drzewietzki, M. Krakowski, I. Krestnikov, and S. Breuer, "Mode locking in a tapered two-section quantum dot laser: design and experiment," Opt. Lett. **43**(12), 2827–2830 (2018).